Proceedings of OMAE'02
21st International Conference on Offshore Mechanics and Arctic Engineering
June 23-28, 2002,Oslo, Norway

OMAE2002-28536

COUPLED DYNAMIC ANALYSIS OF A MINI TLP: COMPARISON WITH MEASUREMENTS

Xiaohong Chen
Ocean Engineering Program
Department of Civil Engineering
Texas A&M University
College Station TX 77843-3136 USA
xiaohong-chen@neo.tamu.edu

Jun Zhang
Ocean Engineering Program
Department of Civil Engineering
Texas A&M University
College Station TX 77843-3136 USA
Jun-Zhang@tamu.edu

Pierre-Yves F. Liagre
Ocean Engineering Program
Department of Civil Engineering
Texas A&M University
College Station TX 77843-3136 USA
Pierre-Liagre@neo.tamu.edu

John M. Niedzwecki
Ocean Engineering Program
Department of Civil Engineering
Texas A&M University
College Station TX 77843-3136 USA
j-niedzwecki@tamu.edu

Per Teigen
Statoil Research Center
Postuttak
N-7005 Trondheim, Norway
pte@satoil.com

ABSTRACT

A numerical code (COUPLE) was recently developed for computing 6 Degree-Of-Freedom (DOF) motions of a moored floating structure dynamically interacting with its mooring/riser/tendon system. The computation of hydro-dynamic forces on the moored structure can be conducted based on a diffraction wave theory model, e.g. WAMIT, and/or the Morison Equation based upon a slender body assumption. Wave kinematics up to the free surface, used in the Morison Equation, is computed using nonlinear deterministic Hybrid Wave Models, and is accurate up to second order in wave steepness. Experimental data from the model tests of a mini TLP was used as the basis for investigation of the numerical computation. Using COUPLE and its alternatives, coupled as well as quasi-static analyses were conducted for the mini TLP model that incorporates four risers and four tendons. Two different methods for computing hydrodynamic loads, namely, WAMIT and Morison Equation, were used, respectively. Through the comparison between the numerical results and the corresponding measurements, dynamic interactions between the riser/tendon system and the hull were examined. Findings made in this study, though based upon a mini TLP may have valuable applications to the design and simulation of a wide range of compliant deep-water structures.

1 INTRODUCTION

Motions and tendon tensions of a Tension Leg Platform (TLP) in severe ocean environment were the focus in many previous studies (Paulling & Webster 1986, Nielsen, et. al. 1994, Davies, et. al. 1994, Kanda, et. al. 1998, Ma, et. al. 2000, Kim, et. al. 2001). It was noticed that dynamic interaction between the hull of a TLP and its tendons is significant. In addition, due to its high heave, roll and pitch natural frequencies, the springing and ringing phenomena may occur, which are critical in the fatigue analysis of its tendons.

Our attempt to quantify a floating offshore structure dynamically interacting with its mooring/tendon/riser system commenced several years ago. A numerical code (SMACOS) was initially developed for computing the 3-DOF motions of a SPAR restrained by mooring lines based on a quasi-static analysis (Cao 1996, Cao and Zhang 1997). The code was later extended to allow for computing the 3-DOF motions of a moored SPAR dynamically interacting with its mooring-line system (Chen et. al. 1999), and recently was improved to include 6-DOF motions of a moored structure. The code, named as COUPLE, consists of two basic codes: one for computing the dynamics of a mooring/tendon/riser system and the other for the wave/current/wind loads on the corresponding floating

structure (hull). The two independent codes are coupled by matching the forces and displacements of the mooring/tendon/riser system and the corresponding floating structure at their joints according to their connection conditions. The code for quantifying dynamics of the mooring-line/riser/tendon system is based on the slender-body assumption and a nonlinear Finite Element Method (FEM), known as CABLE3D (Ma & Webster, 1994). The computation in the original CABLE3D employs the assumption of infinitesimal elongation of a slender rod (mooring /tendon /riser). Because large elongation slender rods, such as springs and synthetic ropes are often used in either a mooring-line model test or a prototype mooring system in deep water, the code of CABLE3D was recently improved to allow for the large elongation of segments in a mooring line to achieve accurate simulation of mooring-line dynamics (Chen et al. 2001a). The computation of nonlinear wave forces on a floating structure is accomplished by using either WAMIT and/or the Morison Equation. While WAMIT is based on a second-order diffraction wave theory and neglects the viscosity of water, the Morison equation is based on the slender-body assumption and employs empirical coefficients for computing the added mass and drag forces. Irregular wave kinematics (input to the Morison Equation) is calculated up to the free surface and accurate to second order in wave steepness based on nonlinear deterministic Hybrid Wave Models (HWM) (Zhang et. al, 1996, 1999).

Extensive model tests of a mini TLP were conducted in the wave basin of Offshore Technology Research Center (OTRC) at Texas A&M University to quantify its wave loads, airgap, motion responses, and tensions in its tendons and risers. The mini TLP was designed for the offshore of West Africa with a relatively benign wave environment. In this study, the newly improved COUPLE and its alternatives were used to calculate the motions of the mini TLP and tensions in its tendons and risers given the incident wave conditions. The numerical results were then compared with the corresponding measurements. The comparison reveals dynamic interactions between the hull of the mini TLP and its riser/tendon system, especially in low frequency (LF) range.

2 GOVERNING EQUATIONS AND FORMULATIONS

2.1 MOTION EQUATIONS

The coordinates are defined in Figure 1, where the X- and Y-axis are located in plane parallel to the calm water surface and the Z-axis is positive upward. The incident wave train is in the direction of the X-axis.

The nonlinear 6-DOF motion equations for a rigid body with respective to an arbitrary point 'o' on the body were derived following the work by Paulling and Webster, (1986), and Lee (1995).

$$m\frac{d^2x}{dt^2} + mT^t(\frac{dw}{dt}\times r_g) + mT^t(w\times(w\times r_g)) = \hat{F} \qquad (1)$$

$$I_o\frac{dw}{dt} + w\times I_o w + mr_g\times(T\frac{d^2x}{dt^2}) = M_o \qquad (2)$$

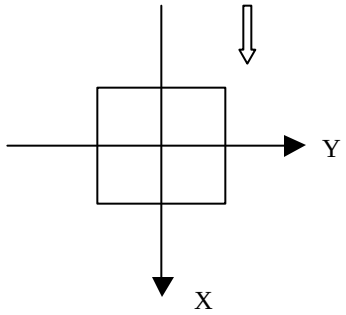

Figure 1 Coordinate System

where the superscript *t* denotes the transpose of a matrix; *m,* is the mass of the structure. $x = (x_1, x_2, x_3)^t$, is the coordinates of the point *o* in the (OXYZ) coordinates fixed on the earth, and $\hat{a}_o = \frac{d^2x}{dt^2}$ is its linear acceleration. $w = (w_1, w_2, w_3)^t$, is the angular velocity with respective to the (*oxyz)* coordinates fixed on the rigid body and $r_g = (x_g, y_g, z_g)^t$, the coordinates of the center of gravity of the body defined in the (*oxyz*) coordinates. I_o is the moment of inertia of the body with respect to the coordinates *oxyz*. $\hat{F}$ is the total forces applied on the body. M_o is the total moments applied on the body with respect to the coordinates *oxyz*. T is the transfer matrix between the (*oxyz*) coordinates fixed on the body and the (OXYZ) coordinates fixed on the earth, which is an orthogonal matrix of the property that $T^t = T^{-1}$.

2.2 HYDRODYNAMIC FORCES ON THE HULL

Forces applied on the hull are computed using two different approaches, as outlined in the following two subsections.

2.2.1 MORISON EQUATIONS WITH HWM

When $l/D>5$, the Morison Equation can be used for computing hydrodynamic forces on a cylinder, where l is the wavelength and D the diameter of the cylinder. This condition is satisfied for the mini TLP in the testing wave environment. The hull is divided into eight equivalent circular cylinders representing four columns and four pontoons. Added-mass, inertia and drag forces applied on a segment of an increment length (*ds*) along the cylinder in the direction normal to the axis of the cylinder are computed by,

$$dF_n = (1+C_m)\rho_f \frac{p}{4}D^2(a_f)_n ds + \frac{1}{2}\rho_f C_D D|v_{rn}|v_{rn} ds - C_m \rho_f \frac{p}{4}D^2 a_n ds, \quad (3)$$

where D is the equivalent diameter of the cylinder. $C_m = C_I - 1$, where C_I is the inertia coefficient and C_m the added-mass coefficient. C_D is the drag coefficient. ρ_f is the density of fluid. v_{rn}, $(a_f)_n$ and a_n are relative velocity, acceleration of the cylinder to ambient fluid and the acceleration of the segment of the cylinder, respectively. The subscript **n** denotes the component of the velocity or acceleration in the direction normal to the axis of the cylinder. Forces applied on the truncated bottom of a cylinder in the axial direction of the cylinder are the summation of the integral of dynamic pressure over the bottom area S_B, drag and added-mass forces. The drag and added-mass forces in the axial direction are caused by the heave of the truncated column.

$$F_t = \iint_{S_B}\left(\rho\frac{\partial(f^{(1)}+f^{(2)})}{\partial t} + \frac{1}{2}\rho|\Delta f^{(1)}|^2\right)n_t ds + \frac{1}{2}\rho_f C_{Dt}\frac{pD^2}{4}|v_{rt}|v_{rt} - C_{mt}\rho_f\frac{4}{3}(\frac{D}{2})^3 a_{rt}, \quad (4)$$

where $f^{(1)}$ and $f^{(2)}$ are first- and second-order potential of incident waves. C_{mt} and C_{Dt} are respectively the added-mass and drag coefficients. v_{rt} and a_{rt} are the relative velocity and acceleration of the bottom of the cylinder with respect to ambient fluid in the axial direction of the cylinder. In Equations (3) and (4), wave kinematics and incident wave potential ($f^{(1)}$ and $f^{(2)}$) are computed using the uni-directional HWM (Zhang, et. al., 1996).

Restoring forces including the hydrostatic and gravity forces are calculated and then stored in a restoring stiffness matrix. Wave radiation and drift damping are neglected in this approach. Mean wave drift forces fail to be computed using the Morison equation. Hence, they are computed based on the results of linear diffraction theory. Since the HWM is accurate up to second order in wave steepness, both sum- and difference-frequency second-order kinematics are included in the resultant wave kinematics.

2.2.2 SECOND-ORDER WAVE DIFFRACTION THEORY

The version of WAMIT 5.3s was based on a second-order wave diffraction theory (WAMIT, 1999). It was used to compute radiation force F_R, wave exciting force F_W, hydrostatic restoring force, and wave-drift damping force applied on the hull.

Radiation force is computed by a convolution shown below. The computation was demonstrated by many studies for linear radiation forces (see, Chitrapu & Ertekin, 1995) and second-order forces (see, de Boom, et. al., 1983, Ran & Kim, 1997).

$$F_R = -\left\{M(\infty)\ddot{x}(t) + \int_{-\infty}^{t} K(t-t')\dot{x}(t')dt'\right\} \quad (5)$$

$$K(t) = \frac{2}{p}\int_0^\infty B(w)\cos(wt)dw \quad (6)$$

$$M(\infty) = A(w) + \frac{1}{w}\int_0^\infty K(t)\sin(wt)dt \quad (7)$$

where w denotes radian wave frequency and $M(\infty)$ the added-mass matrix at infinite wave frequency. $K(t)$ is the matrix of the retardation function, and $A(w)$, $B(w)$ are the added-mass and added-damping matrices at frequency w. The vector, x, denotes the 6-DOF motions of the hull.

Linear wave exciting force was calculated using,

$$F_W^{(1)}(t) = \mathrm{Re}\sum_{j=1}^{N} A_j F^{(1)}(w_j)e^{iw_j t}, \quad (8)$$

and second-order wave exciting force by (Pinkster 1979, Kim & Yue 1991),

$$F_W^{(2)}(t) = \mathrm{Re}\sum_{j=1}^{N}\sum_{k=1}^{N}\left[A_j A_k F^{(2)+}(w_j,w_k)e^{i(w_j+w_k)t}\right] + \mathrm{Re}\sum_{j=1}^{N}\sum_{k=1}^{N}\left[A_j A_k^* F^{(2)-}(w_j,w_k)e^{i(w_j-w_k)t}\right] \quad (9)$$

$F^{(1)}(w)$ is linear transfer function (LTF), while $F^{(2)+}(w_1,w_2)$ and $F^{(2)-}(w_1,w_2)$ are respectively sum-frequency and difference-frequency quadratic transfer function (QTF) of wave exciting force. The superscript * denotes the complex conjugate. Equation (9) accounts for the mean, sum- and difference-frequency second-order wave forces. A_j is the complex amplitude of jth wave component of frequency w_j. It is obtained through the Fast Fourier Transform (FFT) of measured wave elevation or from a target wave spectrum in terms of $\sqrt{2S(w)\Delta w}\,e^{ie_j}$, where $S(w)$ and e_j are respectively the power spectrum and the random phase of jth wave component.

Mean drift force is calculated using,

$$F_{mean} = \sum_{j=1}^{N} A_j^2 F^{(2)-}(w_j,w_j) = 2\int_0^\infty S(w)F^{(2)-}(w,w)dw \quad (10)$$

The spectrum of slow drift force (difference-frequency forces) is given by,

$$S_F(w) = 8\int_0^\infty S(m)S(m+w)\left|F^{(2)-}(m,m+w)\right|^2 dm, \quad (11)$$

and that of the sum-frequency force by,

$$S_F(w) = 8\int_0^{\frac{w}{2}} S(\frac{w}{2}+m)S(\frac{w}{2}-m)\left|F^{(2)+}(\frac{w}{2}+m,\frac{w}{2}-m)\right|^2 dm \quad (12)$$

The wave drift damping coefficients were computed following Clark, et. al. (1993) and Neilsen et. al. (1994).

$$
\begin{aligned}
B_{xx}^{WD}(w,b) &= (\frac{w^2}{g}\frac{\partial F_{dx}}{\partial w} + \frac{4w}{g}F_{dx})\cos b - \frac{2w}{g}\frac{\partial F_{dx}}{\partial b}\sin b, \\
B_{xy}^{WD}(w,b) &= (\frac{w^2}{g}\frac{\partial F_{dx}}{\partial w} + \frac{4w}{g}F_{dx})\sin b + \frac{2w}{g}\frac{\partial F_{dx}}{\partial b}\cos b, \\
B_{yx}^{WD}(w,b) &= (\frac{w^2}{g}\frac{\partial F_{dy}}{\partial w} + \frac{4w}{g}F_{dy})\cos b - \frac{2w}{g}\frac{\partial F_{dy}}{\partial b}\sin b, \\
B_{xy}^{WD}(w,b) &= (\frac{w^2}{g}\frac{\partial F_{dy}}{\partial w} + \frac{4w}{g}F_{dy})\sin b + \frac{2w}{g}\frac{\partial F_{dy}}{\partial b}\cos b,
\end{aligned}
\qquad (13)
$$

where F_{dx} and F_{dy} are the mean wave drift force coefficients at frequency w of surge and sway motions, respectively. b denotes the wave incident angle. The mean wave drift damping forces are computed in a similar way to the mean wave drift forces given in Equation (10). Viscous drag forces applied on the hull cannot be accounted by WAMIT and are calculated using the Morison equation.

2.3 COUPLING WITH TENDONS/RISERS

Two different approaches, namely quasi-static and coupled dynamic analyses are used to account for the interactions between tendons/risers and the hull. In a quasi-static analysis, only the force resulting from the static displacements of a tendon/riser system is applied on the hull while the forces induced by the motions of the tendon/riser system and its interaction with ambient fluid are neglected. This approach has been widely used and its details are omitted for brevity.

In a coupled dynamic analysis, the equations for the motions of the hull and those for the motions of tendons/risers are related by appropriately matching forces and displacements at each time step at the connections or joints of the hull and tendons/risers system. Given the displacements of a tendon/riser at its connection with the hull as a function of time, the dynamic differential equations for a slender rod of prescribed characteristics (such as, the shape, density, bending moment, axial stiffness of the rod and its connection to the sea bottom) can be numerically solved in the time domain using a finite element method and time-domain integral scheme. Hence, the total forces of all tendons and risers applied on the hull at each time step can be computed. They together with the wave loadings on the hull determine the displacements of the hull as a function of time. In this way, the motions of the hull and dynamics of the tendon/riser system can be calculated. Since dynamic equations for the riser/tendon system and hull are solved in this manner, the damping effects of risers and tendons on the hull are included in the coupled analysis.

3 EXPERIMENT SET-UP

The scale of the mini-TLP model to the prototype is 1:40. Comprehensive tests were conducted on a compliant mini-TLP model. In this paper, we only report the comparison between the measurements in a heading sea and the related numerical predictions. Therefore, the description given below is limited to this set of tests. A detailed and complete description of the model tests of the mini TLP was given in the OTRC report (Liagre, 2000). The mini-TLP model has four risers and four tendons, located at four corners of the model as sketched in Figure 2. A spring was inserted in the middle of each riser and tendon model in order to match the axial stiffness of the prototypes. The lower and upper ends of risers and tendons are hinged to the floor of the wave basin and the hull, respectively. Table 1 shows the properties of as-built mini TLP in full scale. It should be noted that the results presented hereafter are all expressed in full scale. The tensions in all tendons and risers were measured at their bottom. The 6-DOF motions of the hull were measured with respect to its center of gravity (CG). Long-crested irregular waves were generated according to a target wave spectrum and wave elevation was measured by 6 wave gages in the absence of the model. The elevation measured at Gage 3 was used in the computation of wave forces. Its location is marked in Figure 2. Free decay tests of the 6-DOF motions of the mini TLP were performed. The related natural periods and critical damping ratios were obtained based on these tests and are given in Table 2. The properties of four risers and four tendons are summarized in Table 3. The length of risers is 667.5m, tendons 629.4m, the height of attachment point above keel of risers is 42.2m, tendons 3.8m, and the diameter of risers is 1.339m, tendons 1.016m, respectively, in full scale.

Properties	As-Built, Full Scale Value	Unit
Water depth	673.61	m
In-place draft	28.51	m
Column diameter	8.64	m
Pontoon height	6.22	m
Pontoon width	6.22	m
Column center-to-center	28.51	m
Total weight of mini-TLP	6445	Metric ton
Vessel displacement	10158	Metric ton
Tendon & riser pretension	3713	Metric ton
Center of Gravity (X)	0	m
Center of Gravity (Y)	0	m
Center of Gravity (Z)[1]	29.5	m
Pitch radius of gyration[2]	21.7	m
Roll radius of gyration[2]	21.9	m
Yaw radius of gyration[2]	17.2	m

[1] above keel

[2] radii of gyration were slightly changed when adjusting tension in tendons and risers.

Table 1 Mini-TLP Properties (As-Built, Full Scale)

	Natural Period [s]	Critical Damping Ratios [%]
Surge	139.97	19.27
Sway	135.55	10.31
Heave	2.79	0.77
Pitch	4.58	1.66
Roll	4.56	1.66
Yaw	101.04	8.05

Table 2 Measured Natural Periods and Critical Damping Ratios

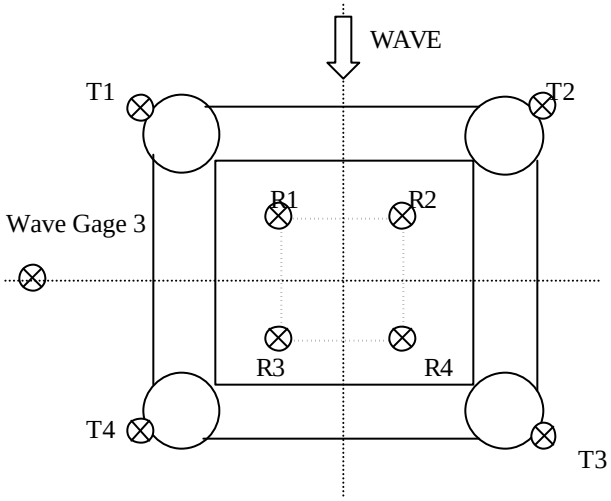

Figure 2 Locations of Tendons (T1-T4) and Risers (R1-R4)

	Pretension		Wet Weight	Axial Stiffness
	@Platform [KN]	@Seafloor [KN]	[KN]	[N/m]
Riser #1	6378.7	2324.6	4054.1	1.118E+07
Riser #2	6387.6	2327.7	4059.9	1.118E+07
Riser #3	6427.7	2350.9	4076.8	1.121E+07
Riser #4	6409.9	2266.4	4143.5	1.120E+07
Tendon #1	2726.8	2413.9	312.9	6.159E+06
Tendon #2	2695.6	2405.0	290.6	6.124E+06
Tendon #3	2704.5	2416.0	288.5	6.130E+06
Tendon #4	2686.7	2361.0	325.5	6.169E+06

Table 3 As Built Risers and Tendons Properties (Full Scale)

4 NUMERICAL SIMULATIONS AND DISCUSSIONS

The target wave spectrum was chosen to simulate a 100-year West Africa stormy sea. It is a JONSWAP type spectrum of a peakness factor of 2.0, peak period of 16s, and significant wave height of 4m. The long crested irregular wave train was advancing in the direction of the X-axis (0 degree heading). The wave spectrum measured at Gage 3 is shown in Figure 3.

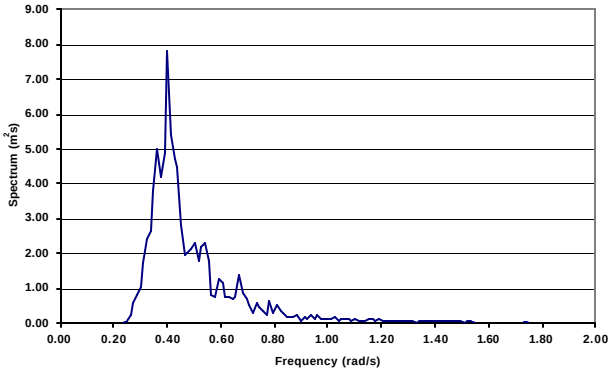

Figure 3 Measured Wave Spectrum (Wave Gage 3)

Numerical simulations of the 6-DOF motions of the hull of the mini TLP and tensions in its tendons and risers were performed using four different approaches.

Approach A is a quasi-static analysis and uses the Morison equation approach for computing wave loads on the hull. Wave kinematics was computed using a uni-directional HWM (Zhang et al. 1996). The duration of the input time series of the wave elevation was about 647 s (a 4096-point segment from measured elevation time series).

Approach B is also a quasi-static analysis but uses second-order WAMIT for computing wave loads on the hull. The drag force on the hull was calculated using the Morison equation in the same way as in Approach A. The duration of the input time series of the wave elevation was the same as in Approach A.

Approach C is also a quasi-static analysis and uses second-order WAMIT for computing wave loads on the mini-TLP. In this approach, the drag force on the hull was neglected and the simulation was much longer, about 3 hours.

Approach D is a coupled dynamic analysis and uses second-order WAMIT for computing wave loads on the hull, which is one of the choices of COUPLE. Same as in Approach C, the drag force on the hull was neglected and the simulation was about 3 hours long.

A 4096-point segment from the measured elevation was used for the computation of wave kinematics, which in turn was used as input to the Morison equation for computing both wave-induced inertia and drag forces on the hull in Approach A and only drag force in Approach B. The same time segment was also used as input to WAMIT for the computation of potential wave loads on the hull in Approach B. Because the time duration (about 647 s) was relatively short to the typical period of Low Frequency (LF) surge motion, dynamic coupling effects between the tendon/riser system and hull cannot be accurately depicted in the simulation. That is why a simple quasi-static analysis was adopted in Approaches A and B. The comparisons among the predictions of Approaches A and B, and the related

measurements may divulge whether or not the wave diffraction is negligible in computing wave forces on the hull and the coupled dynamic interactions between the hull and tendons/riser system are crucial in Wave Frequency (WF) range.

Each riser and tendon was divided into 10 elements. Their drag and added-mass coefficients were set to be unit. In using the Morison equation to compute the wave loads on the hull, the hull was divided into eight elements. Four cylinders of 8.64 m in diameter and 43.5 m in length represent the four vertical columns, and four cylinders of 7.02 m in diameter and 19.935 m in length stand for the four pontoons. Guichard (2001) calculated the horizontal wave forces on the rigid mini-TLP hull (with no tendons and risers) using the Morison equation and linear wave kinematics. By matching his calculation with the corresponding measurements, he adopted Cm=1.0 for the vertical columns and Cm=1.5 for the pontoons. Teign and Niedzwechi (1998) recommended Cd=0.7 for the columns and Cd=1.2 for the pontoons when the mini TLP is in 0-degree heading sea. The above added-mass and drag coefficients were adopted in this study. In addition, we empirically used Cm=1.0 and Cd=3.0 for the heave motion of four vertical columns.

The hull was discretized into 1474×4 panels in using WAMIT. A numerical test was performed concerning whether or not the numbers of panels used was sufficient. It was shown that the mean-drift force computed based on the pressure integration over the hull converges to that computed based on the momentum conservation principle. The stiffness matrix accounting for the restraints of the tendons and risers to the hull was included in the computation using WAMIT as an external stiffness matrix. It was noted that the results for the RAOs of heave, pitch and roll of the hull obtained using WAMIT could be quite different if stiffness of tendons and risers were not included. The coefficients of wave-drift damping were computed based on Equation (13).

The spectrum of second-order difference-frequency surge force applied on the hull under impact of the West Africa Storm is given in Figures 4. The corresponding spectra of first-order and second-order sum-frequency pitch moment are plotted in Figures 5 and 6, respectively. The shape of the first-order surge force spectrum is very similar to that of the wave spectrum. It has a peak magnitude in the order of 10^{13} N^2s. As shown in Figure 4, the peak magnitude of second-order difference-frequency spectrum of the surge force is about 10^{-4} of that of first-order surge force spectrum. Near the resonant surge frequency range, second-order difference-frequency surge force obtained based on Newman's approximation is smaller than that obtained using full Quadratic Transfer Function (QTF) given by WAMIT. Hence, the full QTF from WAMIT was used in the following time-domain simulations. The peak of second-order sum-frequency spectrum for the pitch moment is also about 10^{-4} of that of the corresponding first-order spectrum. As shown in Figure 5, first-order pitch moment spectrum has a minor peak at around 1.4 rad/s. Although its magnitude is about 10^{-2} times of that of the major peak at 0.4 rad/s, this minor peak is much greater in magnitude than the peak in second-order pitch moment spectrum.

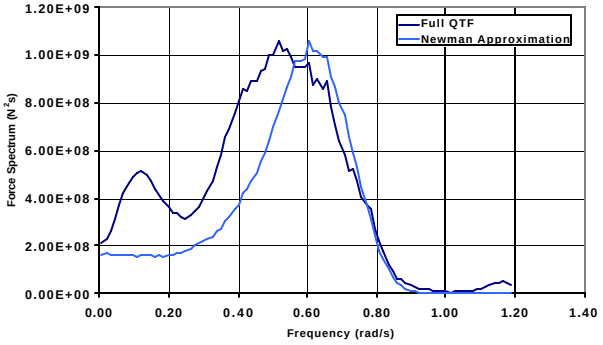

Figure 4 2nd-order Difference-Frequency Wave Force Spectra (Surge)

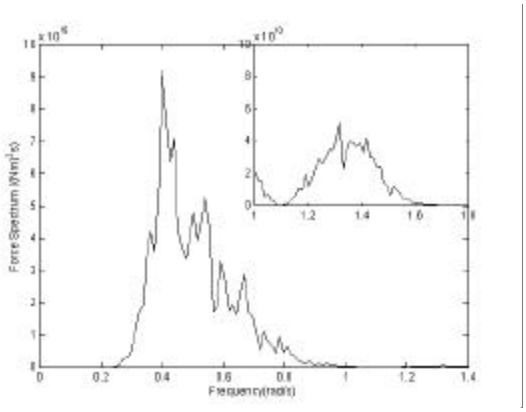

Figure 5 1st-order Wave Force Spectrum (Pitch)

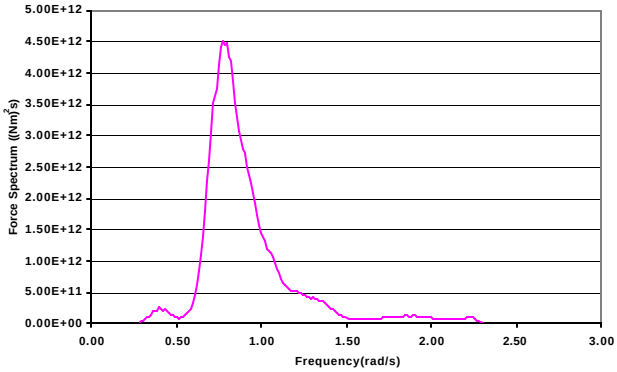

Figure 6 2nd-order Sum-Frequency Wave Force Spectrum (Pitch)

The spectra of surge, heave, pitch motions calculated using Approaches A and B respectively are compared with the corresponding measurements in Figures 7-9. Because these spectra were calculated based on the simulations of 647 s, LF surge motion might not be accurately evaluated. The comparisons show that in the WF range, the motions calculated

using Approach A (Morison equation) is in general similar to those given by Approach B (WAMIT). Both of them are also in satisfactory agreement with the corresponding measurements. It is also noticed that the WF surge motion given by Approach B matches the corresponding measurement slightly better than that of Approach A.

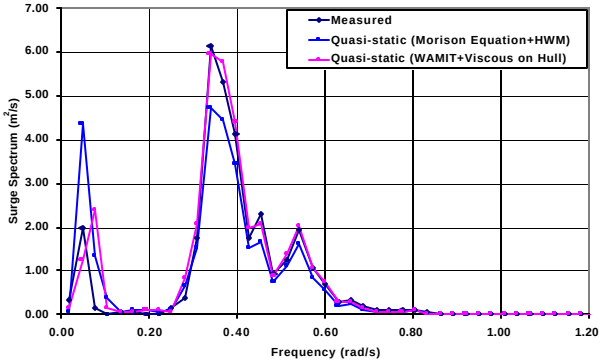

Figure 7 Comparison of Surge Spectra (based on 647s time series)

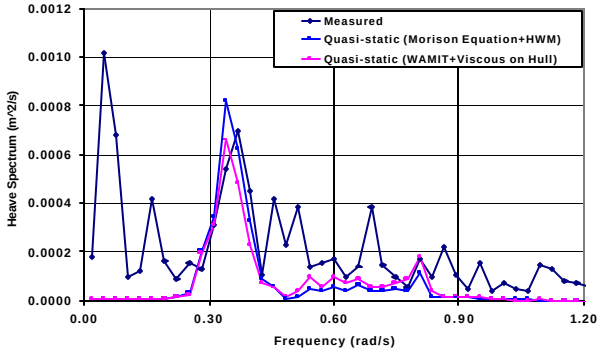

Figure 8 Comparison of Heave Spectra (based on 647s time series)

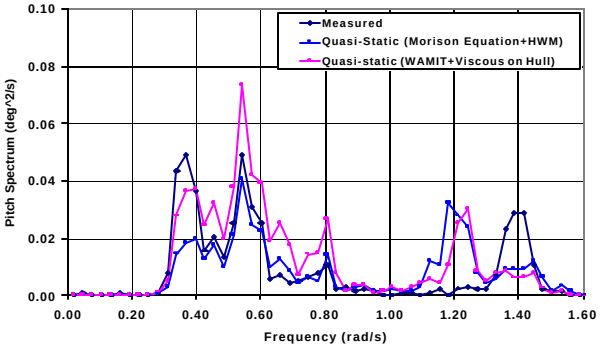

Figure 9 Comparison of Pitch Spectra (based on 647s time series)

The spectra of surge, heave and pitch motions obtained using Approaches C and D are compared with the corresponding measurements in Figures 10-12. It should be noticed that the spectra in these figures were based on 3-hour simulations and viscous drag force on the hull is neglected in both approaches. For the surge motion in WF range, the results obtained using the coupled analysis (Approaches D) and quasi-static analysis (Approach C) are in excellent agreement with the corresponding measurements. Because the damping effects of tendons and risers were excluded in the quasi-static analysis, Approach C greatly over-predicted the LF surge (in comparison with the measurements) while the coupled analysis (Approach D) slightly under-predicted the LF surge. This comparison indicates the dynamic interaction between the tendons/risers and hull may significantly reduce the LF surge motion of the hull. Figure 11 shows that the predicted heave by both approaches are in satisfactory agreement with the measurements in the WF range. However, only Approach D (coupled analysis) rendered satisfactory comparison with the measurements in the LF range while the quasi-static analysis (Approach C) completely missed the heave in the LF range. It should be noted that the overall heave of the TLP is relatively small (roughly 0.04 m). The LF heave was likely induced by the LF surge. Figure 12 shows that the measured resonance frequency of the pitch is slightly higher than the corresponding prediction. The mismatch is probably due to the slightly softer pitch stiffness of the mini TLP used in the computation than the actual pitch stiffness in the tests.

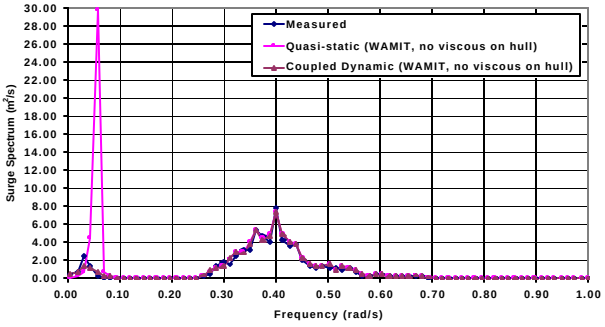

Figure 10 Comparison of Surge Spectra (based on 3 hour time series)

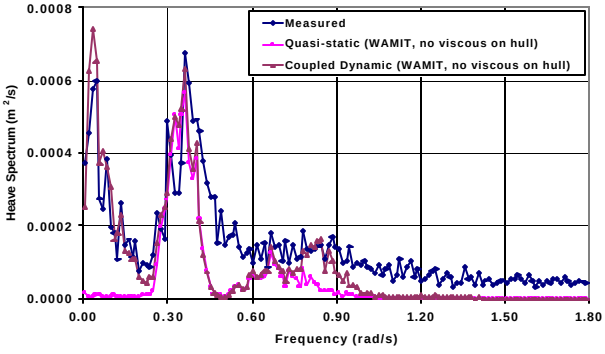

Figure 11 Comparison of Heave Spectra (based on 3 hour time series)

The spectra of measured and computed tensions in tendons and risers are compared in Figures 13-16. Because of the symmetry of the mini TLP with respect to the X-axis and the 0 degree heading sea, only tensions in one front and one rear riser and tendon are presented in the comparison. In general, the predictions are in satisfactory agreement with the corresponding measurements in both LF and WF ranges. Comparing the spectra of surge, heave and pitch motions of the hull with those of tensions, it is found that the tensions in the High Frequency (HF, $0.12<\omega<0.14$ rad/s) range are mainly caused by the pitch of the hull. Because the predicted pitch natural frequency is slightly below the measurement in Figure 12, the predicted peak of the tensions in the HF range is also slightly below the corresponding measurement. It is also noticed that the predicted tension in the HF range is much smaller than the corresponding measurement. The discrepancy between the predicted and measured tensions in the HF range is much greater than that between predicted and measured pitch of the hull.

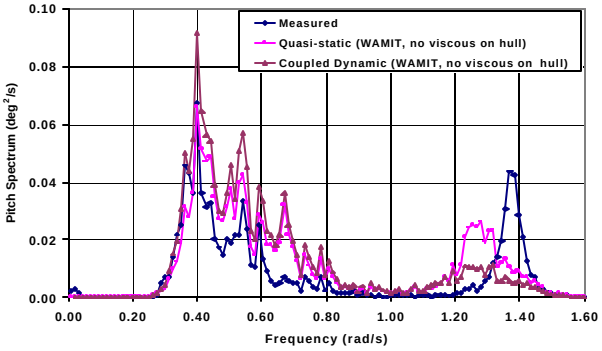

Figure 12 Comparison of Pitch Spectra (based on 3 hour time series)

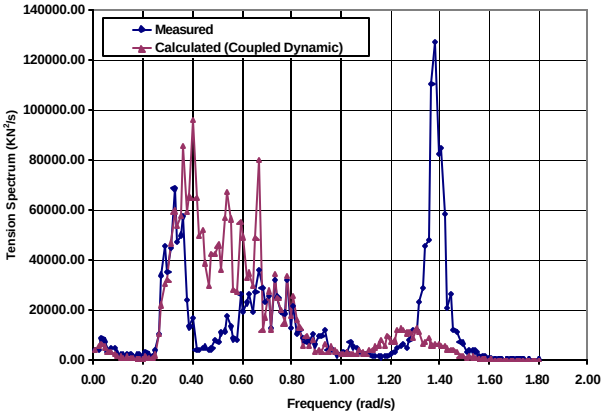

Figure 13 Comparison of Tension (Riser #1, Bottom)

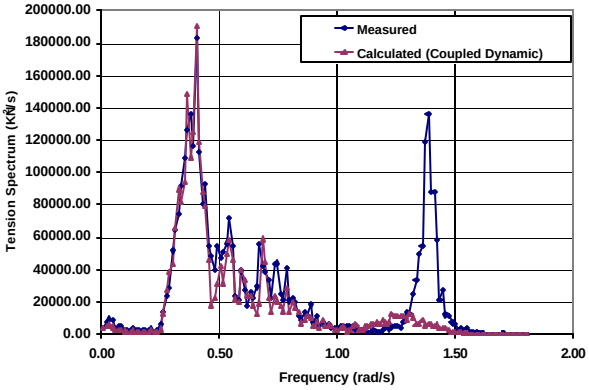

Figure 14 Comparison of Tension (Riser #3,Bottom)

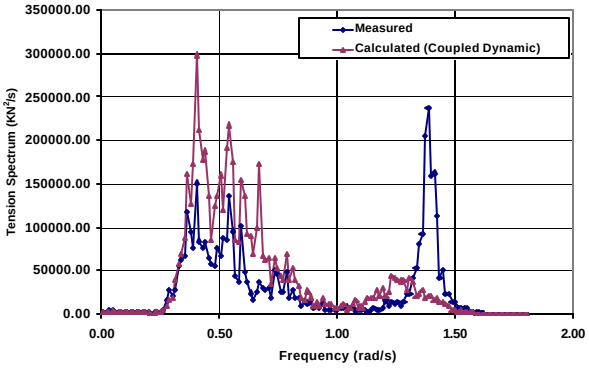

Figure 15 Comparison of Tension (Tendon #1, Bottom)

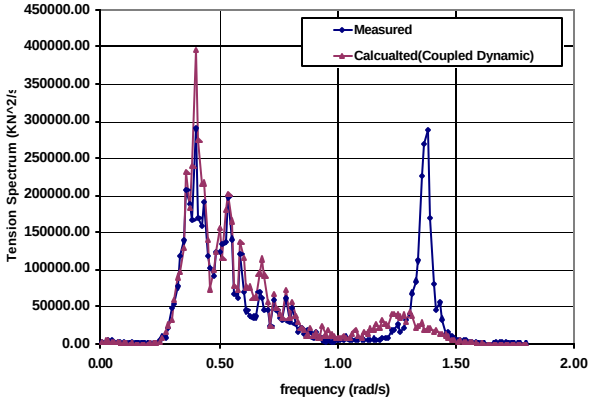

Figure 16 Comparison of Tension (Tendon #4, Bottom)

5 CONCLUSIONS

The following conclusions may be drawn from the comparisons between numerical simulations and laboratory measurements of the mini TLP.

1. Simple computation of wave loads based on the Morison equation but using accurate wave kinematics may render similar results as those given by a relatively sophisticated second-order diffraction wave theory. The simplification

can be allowed if the horizontal dimensions of individual vertical cylinders and pontoons of a TLP are much smaller than the typical wavelength of the incident waves.

2. Quasi-static analysis may provide fairly good prediction of the motions of the hull and tensions in tendons and risers in the WF range. However, it fails to predict the motions in the LF range, while the couple analysis provides satisfactory predictions in both WF and LF ranges.
3. The riser/tendon system provides significant damping to the surge motion of the mini TLP in the LF range, which is consistent with our study on the SPAR (Chen et. al 2001b).
4. Tensions in risers and tendons are dominated by the heave and pitch of the hull. The LF heave can be induced by the LF surge of the hull.

ACKNOWLEDGMENTS

The authors are grateful to the financial support provided by the OTRC at Texas A&M University.

REFERENCES

Liagre, P. (2000), "Mini-TLP 2000 Report", OTRC Report

Cao, P.M. and Zhang, J. (1997), "Slow Motion Responses of Compliant Offshore Structures," *International Journal of Offshore and Polar Engineering*, Vol.7, No.2, 119-126.

Cao, P.M. (1996), "Slow motion responses of compliant offshore structures", *MS Thesis*, Ocean Engineering Program, Civil Engineering Department, Texas A & M University.

Chen, X.H., Zhang, J., Johnson, P. and Irani, M. (2001a), "Dynamic Analysis of Mooring Lines by Using Three Different Methods," ISOPE'01

Chen, X.H., Zhang, J. and Ma, W. (2001b), "On Dynamic Coupling Effects between a Spar and Its Mooring Lines," Ocean Engineering, Vol.28, 863-887

Chen, X.H., Zhang, J. and Ma, W. (1999), "Coupled Analysis of a JIP Spar and Its Mooring System," ISOPE'99

Chitrapu, A.S. and Ertekin, R.C. (1995), "Time-domain Simulation of Large-Amplitude Response of Floating Platforms," *Ocean Engineering*, Vol.22, No.4, 367-385

Clark, P.J., Malenica, S. and Molin, B., (1993), "An Heuristic Approach to Wave Drift Damping," *Appl. Ocean Res.*, Vol.15, 53-55.

de Boom, W.C., Pinkster, J.A. and Tan, S.G. (1983) "Motion and Tether Force Prediction for a Deepwater Tension Leg Platform," OTC4487, 377-388

Faltinsen, O.M. (1990), *Sea Loads on Ships and Offshore Structures*, Cambrifge University Press,U.K.

Garrett, D.L. (1982), "Dynamic analysis of slender rods," *J. of Energy Resources Technology*, Trans. of ASME, Vol. 104, 302-307.

Guichard, A. (2001), "Experimental and Numerical Analysis of a Deepwater Mini-TLP," *MS Thesis (draft)*, Ocean Engineering Program, Civil Engineering Department, Texas A & M University.

Kanda, M., Mlyajima, Nakagawa, H. and Shimazaki K. (1998) "A Nonlinear Coupled Response of TLP Hull and Tendons in Waves," OMAE'98, OMAE98-0472

Kim, M.H., Tahar, A. and Kim, Y.B. (2001) "Variability of TLP Motion Analysis Against Various Design Methodologies/Parameters," ISOPE'01, 467-473

Kim, M.H. and Yue, D.K.P. (1991) "Sum- and Difference-frequency Wave Loads on a Body in Unidirectional Gaussian Seas," *J. Ship Research*, Vol.35, No.2, 127-140.

Lee, C.H. (1995), "Wamit Theory Manual", Report No. 95-2, Massachusetts Institute of Technology 1995

Ma, W. and Webster, W.C. (1994), "An Analytical Approach to cable Dynamics: Theory and User Manual", SEA GRANT PROJECT R/OE-26, September, 1994.

Ma, W., Lee, M.Y., Zou, J., and Huang, E.W. (2000), "Deepwater Nonlinear Coupled Analysis Tool" OTC12085, Houston, Texas

Paulling, J.R. and Webster, W.C. (1986), ``A Consistent, large-amplitude analysis of the coupled response of a TLP and Tendon system," *Proc.of Fifth International Mechanics and Arctic Engineering Symposium*

Pinkster, J.A. (1979), "Mean and Low Frequency Wave Drifting Forces on Floating Structures," *Ocean Engineering*, Vol.6, 593-615

Ran, Z. and Kim, M.H. (1997), "Nonlinear coupled responses of a tethered spar platform in waves," *Intl. J. Offshore & Polar Engr.*, Vol. 7, No. 2, 111-118.

Teigen, P. and Niedzwecki, J.M. (1998) "Experimental and Numerical Assessment of Mini TLP for Benign environments," ISOPE'98, 162-167.

WAMIT, Inc. (1999). "WAMIT User Manual Versions 5.4, 5.4PC, 5.3S"

Zhang, J., Yang, J., Prislin, I., Wen, J., and Hong, K. (1999) "Deterministic Wave Model for Short Crested Ocean Waves, Part I. Theory and Numerical Scheme," *Applied Ocean Research*, Vol. 21, 167-188.

Zhang, J., Chen, L., Ye, M. and Randall, R.E. (1996) "Hybrid Wave Model for Unidirectional Irregular Waves," Part I. Theory and Numerical Scheme, *J. Applied Ocean Research*, Vol. 18, 77-92.